PCCP

ROYAL SOCIETY OF CHEMISTRY

PAPER

View Article Online
View Journal | View Issue

Cite this: *Phys. Chem. Chem. Phys.*, 2021, **23**, 26376

The effect of the composition and pressure on the phase stability and electronic, magnetic, and elastic properties of M_2AX (M = Mn, Fe; A = Al, Ga, Si, Ge; X = C, N) phases†

Vyacheslav S. Zhandun, *[a] Natalia G. Zamkova,[ab] Oksana N. Draganyuk, [a] Aleksey S. Shinkorenko,[a] Ulf Wiedwald, [c] Sergey G. Ovchinnikov[ab] and Michael Farle[ac]

Received 26th July 2021,
Accepted 10th November 2021

DOI: 10.1039/d1cp03427h

rsc.li/pccp

The magnetic properties of M_2AX (M = Mn, Fe; A = Al, Ga, Si, Ge; X = C, N) phases were studied within DFT-GGA. The magnetic electronic ground state is determined. The investigation of the phase stability of M_2AX phases is performed by comparing the total energy of MAX phases to that of the set of competitive phases for calculation of the phase formation enthalpy. As the result of such an approach, we have found one stable compound (Mn_2GaC), and seven metastable ones. It is shown that several metastable MAX phases (Mn_2AlC, Fe_2GaC, Mn_2GeC, and Mn_2GeN) become stable at a small applied pressure (1.5–7 GPa). The mechanical, electronic and elastic properties of metastable MAX phases are studied.

I. Introduction

MAX phases $M_{n+1}AX_n$ (n = 1–3), where M is an early transition metal, A is an A-group element, and X is either carbon or nitrogen[1,2] are hexagonal layered ternary alloys exhibiting a combination of properties of metallic and ceramic materials.[3] MAX phases can be described as $M_{n+1}X_n$ layers stacked in the c direction and separated by single atomic layers of the A element. This layered structure results in a unique combination of physical, chemical, electrical, and mechanical properties.[3] In addition, they have partly been shown and are expected to have anisotropic optical and electronic properties with tunable conductivity in the c direction.[4,5]

Recently, the magnetic MAX phases, containing atoms of chromium, manganese, or iron as an M element, have attracted particular interest. The combination of the layered structure inherent in MAX phases and characteristics such as high stability, high wear resistance, and strong anisotropic properties, with magnetic degrees of freedom, can potentially lead to the emergence of functional materials for various spintronic applications. To date, several magnetic MAX phases as bulk[6–8] as well as thin films[9–13] have been synthesized successfully. However, the problem of finding suitable thermodynamically stable candidates and, therefore, predicting a stable magnetic MAX-phase is still open. Theoretical studies related to MAX phase properties are numerous, ranging from investigations of, *e.g.*, elastic properties to electronic-structure calculations. In particular, the number of magnetic MAX phases was investigated using DFT and evaluation of phase stability and subsequently synthesized.[14–22] However, many MAX phases studied theoretically are not observed experimentally because they turn out to be unstable or metastable. In turn, metastable MAX phases can be stabilized under pressure or in thin films, which is of certain interest. In this work, we perform a systematic investigation of the phase stability based by the method suggested in ref. 23 and 24, of several Mn- and Fe-based magnetic MAX (n = 1) phases (M = Mn, Fe; A = Al, Ga, Si, Ge; X = C, N) using first-principles calculations. For these compounds, the experimental synthesis of Mn_2GaC only has been reported,[11,12] the rest of the studied compounds are hypothetical yet.

The paper is organized as follows. In Section II, we give a short description of the calculation details, in Section IIIA the structural and magnetic properties of Mn- and Fe-based MAX phases are given; in Section IIIB we study the phase stability of the MAX phase; in Section IIIC the effect of the pressure on the phase stability and the elastic and electronic properties of the predicted here metastable MAX phases are given. In the last section, we draw conclusions.

[a] *Kirensky Institute of Physics, Federal Research Center KSC SB RAS, Krasnoyarsk 660036, Russia. E-mail: jvc@iph.krasn.ru*
[b] *Siberian Federal University, 660041 Krasnoyarsk, Russia*
[c] *Faculty of Physics, University of Duisburg-Essen, 47057 Duisburg, Germany*

† Electronic supplementary information (ESI) available. See DOI: 10.1039/d1cp03427h

II. Calculation details

All *ab initio* calculations presented in this paper are performed using the Vienna ab initio simulation package (VASP)[25] with projector augmented wave (PAW) pseudopotentials.[26,27] The valence electron configurations $3d^6 4s^2$ and $3d^5 4s^2$ were taken for Fe and Mn atoms, $3s^2 3p^1$, $3d^{10} 4s^2 4p^1$, $3s^2 3p^2$ and $3d^{10} 4s^2 4p^2$ for Al, Ga, Si and Ge atoms, correspondingly. The calculations are based on the density-functional theory with the Perdew–Burke–Ernzerhoff (PBE) parameterization[28] of the exchange–correlation functional and the generalized gradient approximation (GGA). The plane-wave cutoff energy was 500 eV. We used Monkhorst–Pack grids of special points[29] with the same *k*-points density (parameter KSPACING = 0.15 in VASP) for the Brillouin-zone integration of MAX phases and competing phase (see ESI† for the details of convergence tests). The energy convergence criteria were 10^{-5} eV and 10^{-4} eV for electronic and ionic relaxations, correspondingly. To study phase stability of MAX phases we took the most stable competing phases available in the Materials Project phase diagrams.[30] All phases were optimized with respect to lattice parameters, as well as atomic coordinates for the lowest energy magnetic configurations from Materials Project database.[30] Different magnetic configurations of MAX phases were checked and the configuration with the lowest total energy was included in the study. A linear optimization procedure[23,31] was then used to identify the set of most competing phases with respect to each MAX phase. The formation enthalpy H_{cp} (per atom) is calculated with respect to the identified most competing phases (cp) at zero pressure and temperature. The phonon spectra were calculated using the finite displacement method as implemented in the PHONOPY package[32] with the force matrix obtained from DFT calculations. Structural optimizations were performed for all structures, including lattice parameters and internal coordinates.

III. Results and discussion

A. The structural and magnetic properties

The general crystal structure of the M_2AX phase is shown in Fig. 1. The structure is characterized by a hexagonal unit cell with space group $P6_3/mmc$, containing atomic layers of elements M, A and X, stacked along the *c* direction. Each layer of X atoms is sandwiched between two layers of M atoms, with the X atoms filling the octahedral sites between M-elements. These slabs separate single atomic layers of elements A, with layer A forming a mirror plane in the crystal.

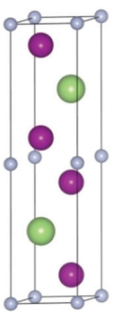

Fig. 1 Crystal structure of M_2AX phase. M, A, and X atoms are shown by purple, green, and grey balls, correspondingly.

To obtain the magnetic ground state of MAX phases, we have calculated the total energies of different magnetic orderings: ferromagnetic (FM) (Fig. 2a) and several types of antiferromagnetic ordering as within unit cell (Fig. 2b–d) as well within cells extended out-of-plane (Fig. 2e–h) and in-plane (Fig. 2i and j). Let us firstly consider the antiferromagnetic configurations realized within the unit cell. At the first type of antiferromagnetic ordering (AFM-I) magnetic moments of the neighboring iron or manganese atoms have the opposite direction along the *c*-axis (Fig. 2b). At the second type of antiferromagnetic ordering (AFM-II) atoms near the middle plane are opposite to the ones near the cell edge (Fig. 2c). At the AFM-III type of magnetic ordering, the magnetic moments of the atoms are oppositely directed relative to the mirror plane of the cell (Fig. 2d). However, as was shown in ref. 12 it is necessary to go beyond the unit cell to consider some antiferromagnetic configurations in the cells extended in-plane and out-of-plane. We have considered here cells doubled (Fig. 2e and f) and tripled

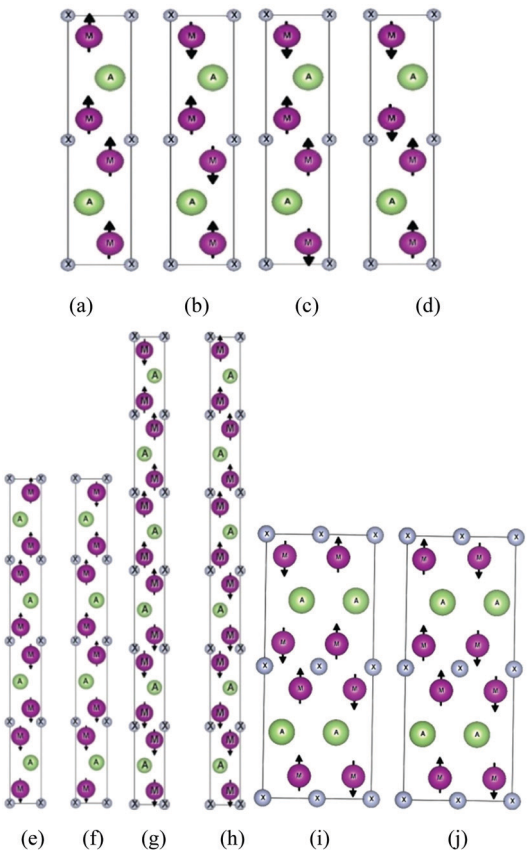

Fig. 2 The possible types of magnetic configurations in M_2AX phases: (a) FM, (b) AFM-I, (c) AFM-II, (d) AFM-III, (e) AFM$[0001]^{X}_{4}$, (f) AFM$[0001]^{A}_{4}$, (g) AFM$[0001]^{A}_{6}$, (h) AFM$[0001]^{X}_{6}$, (i) in-AFM1, (j) in-AFM2. M, A, and X atoms are shown by purple, green, and grey balls, correspondingly. AFM configurations within extended cells are denoted following ref. 12.

Table 1 The obtained magnetic ground state (GS) for all MAX phases, magnetic moments on Mn and Fe atoms ($\mu_{Mn/Fe}$) in the GS and the energy (eV) of the different magnetic configurations. The energy of the GS is taken as zero. AFM configurations within extended cells are denoted following ref. 12

M_2AX	GS	$\mu_{Mn/Fe}$	FM	AFM-I	AFM-II	AFM-III	In-AFM1	In-AFM2	AFM$[0001]_4^X$	AFM$[0001]_4^X$	AFM$[0001]_6^A$	AFM$[0001]_6^X$
Mn_2GaN	AFM-I	±1.9	0.119	0.000	0.064	0.157	0.045	0.148	0.092	0.147	0.103	0.143
Mn_2GeN	In-AFM1	±1.7	0.133	0.125	0.03	0.211	0.000	0.165	0.082	0.189	0.101	0.155
Mn_2SiN	AFM-II	±1.6	0.320	0.183	0.00	0.335	0.097	0.203	0.078	0.273	0.103	0.203
Mn_2AlN	AFM-I	±1.8	0.093	0.000	0.009	0.204	0.088	0.161	0.056	0.161	0.069	0.143
Mn_2GaC	AFM$[0001]_4^A$	±2.1	0.008	0.139	0.006	0.076	0.041	0.067	0.000	0.038	0.003	0.029
Mn_2GeC	AFM-I	±1.8	0.076	0.000	0.032	0.124	0.074	0.080	0.055	0.105	0.063	0.095
Mn_2SiC	AFM-II	±1.8	0.065	0.010	0.00	0.179	0.066	0.179	0.027	0.116	0.038	0.101
Mn_2AlC	FM	1.9	0.000	0.124	0.022	0.059	0.037	0.220	0.007	0.016	0.007	0.011
Fe_2SiN	AFM-II	±0.3	0.006	0.005	0.00	0.012	0.005	0.006	0.003	0.003	0.003	0.006
Fe_2GaN	In-AFM2	±0.8	0.020	0.026	0.011	0.023	0.025	0.000	0.017	0.021	0.022	0.030
Fe_2AlN	In-AFM2	±0.7	0.036	0.010	0.012	0.050	0.017	0.000	0.023	0.011	0.032	0.116
Fe_2GeN	AFM-II	±1.0	0.183	0.190	0.00	0.194	0.317	0.394	0.429	0.177	0.238	0.286
Fe_2SiC	AFM-II	±0.8	0.057	0.036	0.00	0.059	0.059	0.059	0.034	0.045	0.041	0.039
Fe_2GeC	AFM-II	±1.0	0.001	0.062	0.00	0.100	0.003	0.008	0.001	0.002	0.002	0.006
Fe_2GaC	AFM-II	±1.2	0.109	0.142	0.00	0.201	0.231	0.200	0.045	0.762	0.071	0.080
Fe_2AlC	AFM-II	±1.2	0.078	0.120	0.00	0.078	0.223	0.185	0.029	0.032	0.045	0.044

out-of-plane (Fig. 2g and h) and also cells expanded in-plane with antiparallel spins within one M layer (Fig. 2i and j). AFM configurations within extended cells are denoted following ref. 12.

Table 1 shows the calculated lowest energy magnetic configuration (GS) of MAX phases and the values of magnetic moment on the Mn and Fe atoms in the GS phase, the difference in the total energy between GS and other magnetic configurations under consideration. As can be seen from Table 1, in most MAX phases, with the exception of Mn_2GaC, Mn_2GeN, Fe_2GaN and Fe_2AlN considered here magnetic configuration with the lowest energy is specified within unit cell. The most of MAX phases have an antiferromagnetic ground state, ferromagnetic order occurs only in Mn_2AlC. Mn_2GaC has the AFM$[0001]_4^A$ antiferromagnetic phase as the lowest energy magnetic configuration, where magnetic moments are changed sign beyond unit cell. At that, the energies of several magnetic phases of Mn_2GaC (AFM-II, AFM$[0001]_4^A$, FM) are very close to the energy of GS: the difference between them is within 0.008 meV (~88 K) only. Such degeneracy of several phases indicates the competition between FM and AFM exchange interactions that results in the experimentally observed non-collinear canted AFM structure at low temperatures.[33] Notice, a similar near-degeneracy between different magnetic phases also observed in Fe_2GeC, Mn_2AlC, Mn_2AlN and Fe_2SiN. At last, in nitrides Mn_2GeN, Fe_2GaN and Fe_2AlN the lowest energy magnetic structure is realized within cells expanded in-plane. Interestingly, the AFM-III, AFM$[0001]_4^X$ and AFM$[0001]_6^X$ configurations most often turn out to be the most unfavorable configurations.

The magnetic moments in our calculation are smaller than the magnetic moment expected in the localized magnetic moment model. In the Heisenberg model of localized electrons with a spin S the local magnetic moment is expected at $T = 0$ to be $\langle S_z \rangle = S$ (this picture is typical for magnetic oxides like Fe_2O_3, $FeBO_3$ *etc.*, while in the itinerant metallic systems $\langle S_Z \rangle = (n_\uparrow - n_\downarrow)/2$ which may be rather small *vs.* nominal S for magnetic insulators. For example, the magnetic moment of Ni is equal to 0.66 μ_B[34] contrary to the nominal value $S = 1$ for the Ni^{2+} ion. The group of weak ferromagnets has even smaller moments, like $ZrZn_2$ with $\langle S_z \rangle$ = 0.15–0.17 μ_B.[35] Therefore, we suggest the presence of itinerant magnetism in the compounds under consideration. Notice, that values of magnetic moments are in agreement with other theoretical calculations.[11,12,36]

Table 2 The lattice parameters c and a, c/a ratio and internal parameter z/c along c-axis of Mn- and Fe based MAX phases in the GS

Mn_2AX	a, Å	c, Å	c/a	z	Fe_2AX	a, Å	c, Å	c/a	z
Mn_2AlC	2.86	12.31	4.30	0.085	Fe_2AlC	2.85	12.16	4.26	0.083
Mn_2SiC	2.86	11.80	4.13	0.090	Fe_2SiC	2.86	11.38	3.98	0.090
Mn_2GaC	2.89	12.39	4.28	0.082	Fe_2GaC	2.89	11.96	4.14	0.082
Mn_2GeC	2.96	11.77	3.97	0.084	Fe_2GeC	2.95	11.51	3.90	0.086
Mn_2AlN	2.87	12.46	4.34	0.082	Fe_2AlN	2.80	12.35	4.41	0.086
Mn_2SiN	2.80	11.96	4.27	0.092	Fe_2SiN	2.78	11.68	4.20	0.094
Mn_2GaN	2.90	12.23	4.22	0.082	Fe_2GaN	2.88	11.93	4.14	0.082
Mn_2GeN	2.89	12.00	4.15	0.087	Fe_2GeN	2.91	11.55	3.97	0.087

The crystal structure is completely determined by the lattice vector a, internal parameter z along c-axis and the c/a ratio. The calculated parameters of cell of lowest energy magnetic configuration – are given in Table 2.

The calculated lattice parameters of Mn_2GaC are close to experimental values (a = 0.29 nm; c = 1.255 nm) obtained from XRD measurements.[11,33] The in-plane lattice parameter a slightly increases when the atomic number of the A-site cation increases and varies within 3% for different compounds. The out-of-plane lattice parameters c change much stronger with a change in composition (~9%) and have the largest value for Al- and Ga-based MAX phases. Notice, that the c/a ratio for nitrides is larger than carbides, *i.e.* nitrides are more anisotropic than carbides.

B. Phase stability

Let us consider the problem of the phase stability of the studied MAX phases. Evaluation of phase stability is a powerful tool for the prediction of new phases, as demonstrated for several well-known ternary carbide and nitride MAX phases.[11,15,20–24]

Table 3 The calculated elastic constants (C_{ij}) and Born–Huang criteria α, β from eqn (1) for the GS of MAX phases

M_2AX	C_{11}, (GPa)	C_{12}, (GPa)	C_{13}, (GPa)	C_{33}, (GPa)	C_{44}, (GPa)	Born–Huang criteria α	Born–Huang criteria $\beta \times 10^{-5}$
Fe_2AlN	253.3	191.4	120.0	253.3	59.2	61.9	0.8
Fe_2SiN	318.6	229.6	206.1	415.0	56.6	89.0	1.4
Fe_2GaN	227.0	128.0	73.0	263.0	67.0	99.0	0.8
Fe_2GeN	247.0	102.0	102.0	308.0	53.0	145.0	0.9
Mn_2AlN	315.5	111.0	95.6	313.2	75.5	204.5	1.2
Mn_2SiN	335.4	154.3	148.9	395.5	74.6	181.1	1.5
Mn_2GaN	272.5	92.1	107.5	305.3	84.5	180.4	0.9
Mn_2GeN	263.7	115.3	118.8	307.8	51.9	148.4	0.9
Fe_2AlC	281.1	96.9	83.3	265.9	80.3	184.2	0.9
Fe_2SiC	201.8	108.5	109.8	329.2	83.2	93.3	0.8
Fe_2GaC	267.5	123.2	115.0	266.8	77.4	144.3	0.8
Fe_2GeC	168.9	103.5	114.9	192.9	67.5	65.4	0.3
Mn_2AlC	225.9	49.4	56.3	214.2	116.3	176.5	0.5
Mn_2SiC	330.4	113.9	128.9	335.8	94.8	216.5	1.2
Mn_2GaC	318.3	118.7	123.0	303.3	90.8	199.6	1.0
Mn_2GeC	316.6	133.0	138.8	335.2	75.4	183.6	1.1
Fe_2AlN	253.3	191.4	120.0	253.3	59.2	61.9	0.8

Our investigation considers whether the calculated compounds can be expected to exist experimentally. Indeed, there are a lot of possible hypothetical MAX phases taking the various atoms at M, A, and X-sites into account. However, not all MAX phases will be stable in practice.

Firstly, we calculated elastic constants and studied the mechanical stability of the MAX phases. VASP directly provides the full set of second-order elastic constants C_{ij}. The elastic tensor is determined by performing six finite distortions of the lattice and deriving the elastic constants from the strain–stress relationship. The obtained values of the elastic constants for GS of MAX phases are given in Table 3.

A necessary (but not sufficient) condition for the stability of this compound is the fulfillment of the Born–Huang criteria[37]

$$\alpha = C_{11} - |C_{12}| > 0 \quad (1)$$

$$\beta = C_{33}\cdot(C_{11} + C_{12}) - 2{C_{13}}^2 > 0$$

As can be seen from the two last columns of Table 3, all compounds satisfy the Born–Huang criteria and, therefore, are mechanically stable.

However, the fulfillment of the criteria for mechanical stability does not mean that the compound will have thermodynamic stability and would exist experimentally. The formation enthalpy calculated in the framework of the common scheme as the total energy minus the energy of the constituent elements:

$$E_f = E(M_2AX) - 2E(M) - E(A) - E(X) \quad (2)$$

usually found to be negative, favoring phase formation. However, this information alone is insufficient to predict the actual existence of the compounds. Indeed, we have calculated formation energies for all compounds under consideration using eqn (2). To calculate total energies of the constituent elements we have used the Material Project database.[30] Since N cannot be treated as an isolated atom, we have calculated N as N_2 (gas phase). According to the calculation, all MAX phases turned out to be stable (Table 5). Notice, the similar calculations of formation enthalpy were performed by[36] and our values of E_f for carbide MAX phases are close to ones obtained in ref. 36.

The most successful approach for evaluating the stability of a MAX phase of certain composition was suggested in the ref. 23 and 24. This method consists of comparing the calculated total energy of MAX phases to that of the competing phases as determined from the ternary phase diagrams:

$$\Delta H_{cp} = E(MAX) - E_{cp}(b^M, b^A, b^X) \quad (3)$$

This process is necessary because, although a particular M_2AX phase may be energetically favorable over the constituent elements, the phase will not appear if it is more energetically favorable to form two or more different compounds instead. Further, we perform the study of the phase stability of M_2AX phases within this method. To select the competing phases, we use a ternary phase diagram available from ref. 30 for each system in the consideration.

In Table 4, the competing phases included in the calculation of formation enthalpy are presented. We used the most thermodynamically stable phases with the formation enthalpy less than 0.1 eV per atom available in ref. 30 as the competitive phase. Following ref. 23, the simplex linear optimization procedure was used to solve the equation for a given elemental composition b^M, b^A, and b^X (eqn (1) in ref. 23). If $\Delta H_{cp} < 0$, the MAX phase is considered to be stable, and if $\Delta H_{cp} > 0$ it is not. Table 5 shows the total energies of the MAX phase, the most favorable combination of competitive phases, and MAX phase formation enthalpies. Note that, although unstable competing phases were used in calculating the formation enthalpy, the set of lowest energy competing phases include only stable compounds.

As can be seen, the most of MAX phases have positive formation enthalpy, which indicates that they are unstable and cannot be observed experimentally; rather it is energetically more favorable to form two or more different compounds with the same composition. Obtained here ΔH_{cp} for Mn_2AlC and Mn_2AlN are in well agreement with ref. 23 where the stability of a number of MAX phases was checked. Note that in ref. 23, as a rule, stable phases are realized as a set of lowest energy competing phases. We obtained that only Mn_2GaC MAX phase has the negative formation enthalpy $H_{cp} = -0.035$ eV per atom. The stability of Mn_2GaC is in accordance with experimental observations and other theoretical predictions.[11,12,33,36] The obtained here value of formation enthalpy H_{cp} for Mn_2GaC is compared to previous work (-0.03 eV per atom in ref. 11). At that, several MAX phases (Mn_2GeC[38], Mn_2AlC, Mn_2GaN, Mn_2GeN, Mn_2SiC, Fe_2GaC and Fe_2AlC) have the low positive formation enthalpy that can be evidence of the metastability of these compounds.

Table 4 The sets of competitive phases including in the phase stability investigation. The magnetic configurations of corresponding phases are given in brackets

MAX phases	Competitive phases
Fe_2AlC	AlFe(FM), $AlFe_3$(FM), $Al_{13}Fe_4$(NM), Al_6Fe(NM), Al_8Fe_5(FM), Al_9Fe_2(FM), $AlFe_2$(FM), Fe^2C(FM), Fe_5C_2(FM), Fe_3C(FM), Al_4C_3(NM), $AlFe_3C$(FM), Fe(FM), Al(NM), C(NM)
Fe_2SiC	Fe_3Si(FM), FeSi(NM), $FeSi_2$(NM), Fe_5C_2(FM), Fe_3C(FM), Fe_2C(FM), Fe(FM), Si(NM), C(NM)
Fe_2GaC	Ga_3Fe(NM), $GaFe_3$(FM), Ga_4Fe_3(FM), Ga_5Fe_6(FM), GaFe(FM), $GaFe_2$(FM), Fe_5C_2(FM), Fe_3C(FM), Fe^2C(FM), GaC(NM), GaC_3(NM), Ga_2Fe_6C(FM), Fe(FM), Ga(NM), C(NM)
Fe_2GeC	Fe_3Ge(FM), FeGe(FM), Fe_5C_2(FM), Fe_3C(FM), Fe_2C(FM), Fe(FM), Ge(NM), C(NM)
Mn_2AlC	$MnAl_6$(NM), MnAl(FM), Mn_4Al_{11}(FiM), Mn_7C_3(FiM), Al_4C_3(NM), Mn_3AlC(FM), $Mn_{23}C_6$(FiM), Mn_5C_2(FM), Mn_3Al_{10}(FM), $MnAl_{12}$(FM), Mn(FM), Al(NM), C(NM)
Mn_2SiC	MnSi(FM), Mn_3Si(FiM), Mn_4Si_7(NM), Mn_7C_3(FiM), SiC(NM), $Mn_{23}C_6$(FiM), Mn_5C_2(FM), Mn(FM), Si(NM), C(NM)
Mn_2GaC	MnGa(FM), $MnGa_4$(FM), Mn_7C_3(FiM), Mn_3GaC(AFM), $Mn_{23}C_6$(FiM), Mn_5C_2(FM), Mn(FM), Ga(NM), C(NM)
Mn_2GeC	Mn_5Ge_3(FM), Mn_3Ge(FM), $Mn_{23}C_6$(FiM), Mn_7C_3(FiM), MnGe(FM), $Mn_{11}Ge_8$(FM), Mn_2Ge(FM), Mn_3Ge_5(FiM), Mn_3GeC(AFM), Mn_5C_2(FM), $MnGe_2$(FM), Mn(FM), Ge(NM), C(NM)
Fe_2AlN	AlFe(FM), $AlFe_3$(FM), $Al_{13}Fe_4$(NM), Al_6Fe(NM), Al_8Fe_5(FM), Al_9Fe_2(FM), $AlFe_2$(FM), Fe_3N(FM), FeN(NM), AlN(NM), Fe(FM), Al(NM), N_2(NM)
Fe_2SiN	Fe_3Si(FM), FeSi(NM), $FeSi_2$(NM), Fe_3N(FM), FeN(NM), Si_3N_4(NM), Fe(FM), Si(NM), N_2(NM)
Fe_2GaN	Ga_3Fe(NM), $GaFe_3$(FM), Ga_4Fe_3(FM), Ga_5Fe_6(FM), GaFe(FM), $GaFe_2$(FM), Fe_3N(FM), FeN(NM), GaN(NM), Fe(FM), Ga(NM), N_2(NM)
Fe_2GeN	Fe_3Ge(FM), FeGe(FM), Fe_3N(FM), FeN(NM), Ge_3N_4(NM), Fe(FM), Ge(NM), N_2(NM)
Mn_2AlN	$MnAl_6$(NM), Mn_4Al_{11}(FiM), MnAl(FM), MnN(NM), Mn_4N(FiM), Mn_2N(FM), AlN(NM), Mn(FM), Al(NM), N_2(NM)
Mn_2SiN	MnSi(FM), Mn_3Si(FiM), Mn_4Si_7(NM), MnN(NM), Mn_4N(FiM), Mn_2N(FM), Si_3N_4(NM), Mn(FM), Si(NM), N_2(NM)
Mn_2GaN	MnGa(FM), $MnGa_4$(FM), MnN(NM), Mn_4N(FiM), Mn_2N(FM), GaN(NM), Mn_3GaN(FM), Mn(FM), Ga(NM), N_2(NM)
Mn_2GeN	Mn_5Ge_3(FM), Mn_3Ge(FM), MnGe(FM), $Mn_{11}Ge_8$(FM), Mn_2Ge(FM), Mn_3Ge_5(FiM), MnN(NM), Mn_4N(FiM), Mn_2N(FM), $Mn_{12}Ge_4N_3$(FM), Mn(FM), Ge(NM), N_2(NM)

The comparison of the formation enthalpy of compounds with different compositions is given in Fig. 3. As seen, Mn-based compounds mostly have the lower H_{cp} than Fe-based MAX phases. At that, the nitride compounds are higher by enthalpy than carbides. A distinctive feature of the dependence of formation enthalpy on atom A is the pronounced minimum for the Ga-based compounds. However, if for carbides the Si-based compounds have the highest enthalpy, then in nitrides the Al-based MAX-phases are the most thermodynamically unstable. One should note the trend that Si rather tends to form silicides with transition metals with the common formula M_3Si (M = Mn or Fe) instead of MAX phases.

C. The elastic, electronic and magnetic properties of metastable MAX phases under pressure

As follows from Table 5 and Fig. 3, seven compounds: Mn_2GeC, Mn_2AlC, Mn_2GaN, Mn_2GeN, Mn_2SiC, Fe_2GaC and Fe_2AlC are metastable and very close to thermodynamic stability with formation enthalpies H_{cp} within 0.1 eV per atom. It can be assumed that these MAX phases can be realized by a small applied pressure. To check this possibility, we have performed the calculation of the formation enthalpies dependence of MAX phases on the isotropic pressure within the described above procedure. We choose the metastable compounds with H_{cp} below 0.1 eV per atom for testing. The results are given in Fig. 4. Notice, the set of competing phases under pressure does not change under the low pressure used here. Indeed, as seen from Fig. 4, Mn_2AlC, Fe_2GaC, Mn_2GeC and Mn_2GeN compounds become stable at pressures $\sim$1.5 GPa, $\sim$5 GPa, $\sim$7 GPa and $\sim$2.5 GPa correspondingly. However, Fe_2AlC, Mn_2SiC, and Mn_2GaN remain unstable up to a pressure of 20 GPa. These results suggest that the quite small pressure supports the stabilization of some metastable MAX phases. In the present calculation we use isotropic pressure, but it can be expected that metastable MAX phases are stabilized at anisotropic pressure as well. Such pressure can be realized by using the lattice mismatch of a MAX phase film grown on a corresponding substrate. In this case, the compounds will experience compression or tension depending on the substrate material, and the applied pressure can stabilize these compounds.

Table 6 shows the elastic constants for Mn_2AlC, Fe_2GaC, Mn_2GeC and Mn_2GeN at a pressure of P = 8 GPa and some elastic properties including the elastic moduli (B, G, E) and Poisson's ratio μ. As reported in ref. 39 the MAX phases do not exhibit significant elastic anisotropy in contrast to other layered solids. This is evidenced in particular by the fact that C_{33} and C_{11} constants are almost equal for the considered compounds. Indeed, C_{33} and C_{11} constants have similar values for carbides Mn_2AlC and Fe_2GaC. It should be noted, that the same is true for some of the M_2AlC phases.[40] Nitride Mn_2GeN is more anisotropic with a ratio between the uniaxial compression values along the c and a axis: $k_c/k_a = (C_{11} + C_{12} - 2C_{13})/(C_{33} - C_{13})$ (Table 6). All compounds have large values for the bulk modulus B and Young's modulus E, which indicates the resistance to volume change and high stiffness of these materials. At the same time, the values of shear modulus G are small, *i.e.* these materials can shape-change quite easily. The Poisson's ratio plays another significant role in evaluating the nature of chemical bonding in solid materials. The Poisson's ratio for a pure covalent crystal has a value of 0.1. Conversely, the completely metallic compounds possess a value of 0.33. As seen in the studied compounds the Poisson's ratio indicates a large contribution of the metallic bonds in the MAX phases.

Of the four compounds realized at low pressure (Mn_2AlC, Fe_2GaC, Mn_2GeC and Mn_2GeN), Mn_2AlC has FM ordering, while in the other three, the antiferromagnetic structure has

Table 5 The total energies (per formula unit) of the MAX phase (E_{MAX}) and the most favorable combination of competitive phases (E_{comp}), formation enthalpies of MAX phase (ΔH_{cp}) in comparison of the competitive phases and formation energies (E_f) obtained from eqn (2)

	E_{MAX}	E_{comp}				E_{MAX}	E_{comp}		
	M_2AlX	Competitive phases	ΔH_{cp}, eV per atom	E_f, eV per atom		M_2SiX	Competitive phases	ΔH_{cp}, eV per atom	E_f, eV per atom
	Fe_2AlC	0.5C + 0.5AlFe + $0.5AlFe_3C$	0.07	−0.39		Fe_2SiC	C + $0.5Fe_3Si$ + 0.5FeSi	0.31	−0.46
E, eV	−29.83	−30.12			E, eV	−31.12	−32.30		
	Fe_2AlN	AlN + 2Fe	0.45	−1.41		Fe_2SiN	$0.24Fe_3N$ + 0.43FeN + $0.19Si_3N_4$	0.33	−5.36
E, eV	−29.01	−30.81			E, eV	−30.48	−31.73		
	Mn_2AlC	0.5MnAl + $0.5Mn_3AlC$ + 0.5C	0.008	−0.22		Mn_2SiC	0.5MnSi + $0.5Mn_3Si$ + C	0.11	−0.81
E, eV	−31.69	−31.72			E, eV	−33.31	−33.71		
	Mn_2AlN	AlN + 2Mn	0.34	−1.64		Mn_2SiN	1.25Mn + $0.25Mn_3Si$ + $0.25Si_3N_4$	0.28	−6.35
E, eV	−31.43	−32.89			E, eV	−32.88	−33.97		

	M_2GeX	Competitive phases	ΔH_{cp}, eV per atom	E_f, eV per atom		M_2GaX	Competitive phases	ΔH_{cp}, eV per atom	E_f, eV per atom
	Fe_2GeC	C + 0.5Fe3Ge + 0.5FeGe	0.15	−0.42		Fe_2GaC	C + $0.125Ga_3Fe$ + $0.625GaFe_3$	0.06	−0.36
E, eV	−29.91	−30.56			E, eV	−28.76	−28.99		
	Fe_2GeN	FeN + FeGe	0.19	−1.23		Fe_2GaN	0.5FeN + $0.5GaFe_3$ + 0.25GaN	0.14	−1.34
E, eV	−29.09	−29.83			E, eV	−27.94	−28.53		
	Mn_2GeC	$0.5Mn_3GeC$ + 0.5C + 0.5MnGe	0.02	−0.12		Mn_2GaC	$0.63Mn_3GaC$ + 0.36C + $0.09MnGa_4$	−0.03	−0.15
E, eV	−32.12	−32.04			E, eV	−30.724	−30.581		
	Mn_2GeN	Mn_2N + Ge	0.025	−1.49		Mn_2GaN	$0.67Mn_3GaN$ + 0.33GaN	0.03	−1.59
E, eV	−31.59	−31.71			E, eV	−30.41	−30.54		

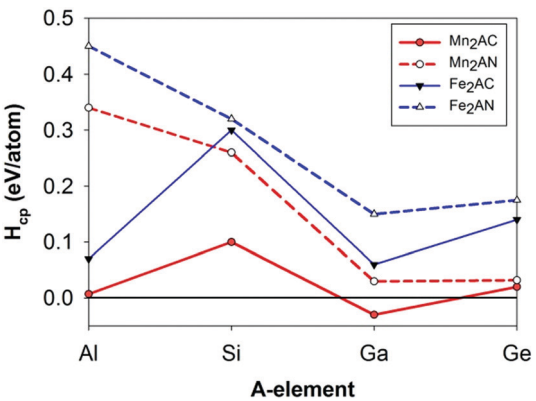

Fig. 3 Calculated formation enthalpies of M_2AX phases with respect to most competing phases in dependence on the composition of M-, A- and X-sites.

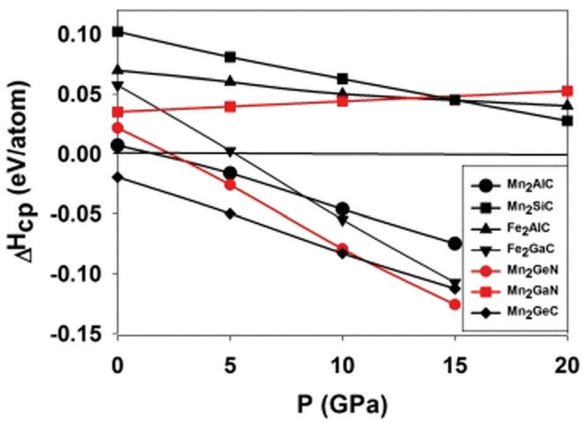

Fig. 4 The stability of MAX phase under pressure: relative formation enthalpy as difference between formation enthalpy of MAX phase and competing phases (ΔH_{CP} = H(MAX) − H(comp. phases)).

the lowest energy. When the pressure of P = 8 GPa is applied, the magnetic moments in these MAX phases practically do not change. In Fig. 5 the DOS of these compounds are given. A common feature of all DOS is the absence of pronounced peaks corresponding to localized electrons. Electronic states are smeared over a wide range of energies, which, along with relatively small values of magnetic moments (Table 1) points

Table 6 The elastic constants (C_{ij}), Born–Huang criteria, bulk modulus (B), shear modulus (G), Poisson's ratio (μ), Young's modulus (E) and k_c/k_a ratio for metastable phases at pressure P = 5 GPa

						Born–Huang criteria						
MAX phases	C_{11} (GPa)	C_{12} (GPa)	C_{13} (GPa)	C_{33} (GPa)	C_{44} (GPa)	α	$\beta \times 10^{-5}$	B (GPa)	G (GPa)	μ	E	k_c/k_a
Fe_2GaC	308.1	149.0	151.0	303.3	79.6	159.1	0.9	202.3	78.9	0.32	209.5	1.02
Mn_2AlC	313.2	145.0	134.1	312.0	84.1	168.2	1.0	196.0	85.4	0.25	223.7	1.07
Mn_2GeN	349.5	174.0	173.0	401.0	87.2	175.5	1.5	237.6	91.0	0.30	242.0	0.78
Mn_2GeC	319.1	117.0	105.6	304.7	101.0	172.1	1.3	221.9	98.7	0.30	251.9	1.10

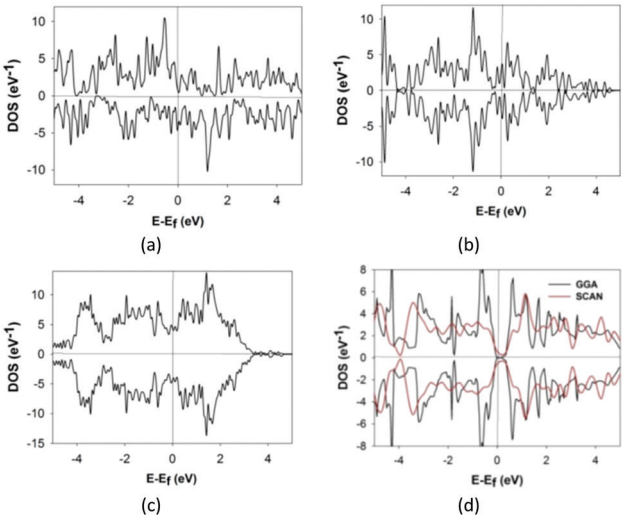

Fig. 5 The density of states of (a) Mn_2AlC, (b) Fe_2GaC (c) Mn_2GeN and (d) Mn_2GeC MAX phases under pressure P = 8 GPa. Negative values of DOS correspond to the minority spin states. Zero on the energy axis corresponds to the Fermi energy.

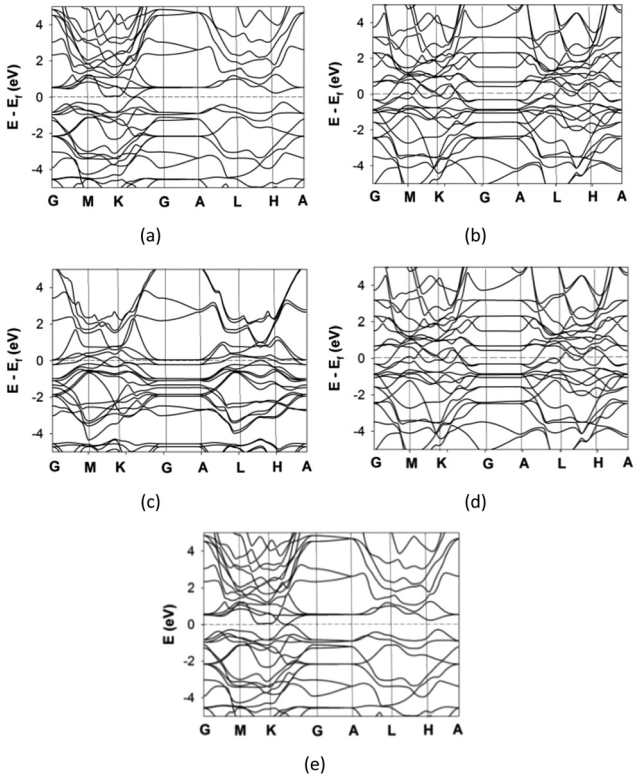

Fig. 6 The band structure of (a) Mn_2AlC (spin up states), (b) Mn_2AlC (spin down states), (c) Fe_2GaC and (d) Mn_2GeN and (e) Mn_2GeC MAX phases under pressure P = 8 GPa. Zero on the energy axis corresponds to the Fermi energy.

at itinerant magnetism in these compounds. The states near the Fermi energy are mainly occupied by Mn/Fe d-electrons.

As seen, three compounds (Mn_2AlC, Fe_2GaC, and Mn_2GeN) are metals (Fig. 5 and 6). As for Mn_2GeC, the behavior of DOS and Poisson's ratio (see Table 6) indicate the metal-like behavior of the compound, however, we obtained that the density of states has a pronounced decrease at the Fermi energy. To check whether this is not a problem with the calculation method, we performed SCAN-based calculation[41] of the density of states. The comparison of DOS within both approaches is given in Fig. 5d. The result obtained with SCAN functionals is in qualitative good agreement with GGA-based calculations and the abrupt decrease at the Fermi energy is observed also. As seen from the band structure (Fig. 6e), this is due to the proximity of the valence and conductive bands nearest to the Fermi energy in the vicinity of the K point of the Brillouin zone (along with MK and KG directions). All band structures (Fig. 6) have the similar behavior: for example, one can see the presence of flat bands in the G–A direction, which is a consequence of the layering of the structure and two-dimensionality of electrons. Note, that in Fe_2GaC and Mn_2AlC (spin-down states only) the flat bands are on the Fermi level. This results in the appearance of the peak at the Fermi energy in DOS (Fig. 5). Since a peak at the Fermi level is a necessary (but not sufficient) condition for the presence of superconductivity in a material, this feature may be interesting from the point of view of potential superconductivity in the above-mentioned MAX phases and requires additional researches.

IV. Conclusions

In summary, we theoretically studied the effect of composition and pressure on the magnetic, electronic and elastic properties and phase stability of Mn- and Fe-based magnetic MAX phases. All studied compounds, except ferromagnetic Mn_2AlC are antiferromagnetic. In all MAX phases, with the exception of Mn_2GaC, Mn_2GeN, Fe_2AlN and Fe_2GaN considered here the magnetic configuration with the lowest energy is specified

within the unit cell. Mn_2GaC has the AFM$[0001]_4^A$ antiferromagnetic phase as the lowest energy magnetic configuration, while in Mn_2GeC, Fe_2GaN and Fe_2AlN magnetic moments are antiparallel within one M layer. We have investigated the phase stability of M_2AX phases using DFT calculations and considered competitive phases to calculate the formation enthalpy of MAX phases in combination with linear optimization procedures. We found that, in agreement with previous calculations,[11,12,36] Mn_2GaC is thermodynamically stable. For both carbon and nitrogen-containing MAX phases, maximum stability is reached around the Ga atom as an A-site element. In addition, we obtained that Fe-based MAX phases are less stable than Mn-based compounds. Our calculation also revealed several metastable phases close to stability which could be stabilized by pressures of 1.5–7 GPa, *i.e.* Mn_2AlC, Fe_2GaC, Mn_2GeC and Mn_2GeN MAX phases. For predicted metastable MAX phases the electronic structure and the elastic properties were calculated and analyzed. We find itinerant magnetism and a dominating metallic bond character for all compounds. All compounds are characterized by a large bulk modulus and small shear modulus. Our method is a reliable tool that can be used as guidance for further search of new MAX phases before time-consuming and expensive experimental investigations, are attempted.

Conflicts of interest

There are no conflicts to declare.

Acknowledgements

The reported study was funded by Russian Foundation for Basic Research, Government of Krasnoyarsk Territory, Krasnoyarsk Regional Fund of Science to the research project no. 20-42-240004: ''The effect of the composition, pressure, and dimension on the magnetic, electronic, optical, and elastic properties of the magnetic $M_{n+1}AX_n$ (M = Cr, Mn; Fe, A = Al, Ga, Si, Ge, P, In; X = C, N; n = 1–3) MAX-phases'' and by the Government of the Russian Federation (agreement no. 075-15-2019-1886). The calculations were performed with the computer resources of ''Complex modeling and data processing research installations of mega-class'' SRC ''Kurchatovsky Institute'' (http://ckp.urcki.ru). The ternary phase diagrams for the calculation of formation enthalpies were taken from Materials Project (https://materialsproject.org). U. W. and M. F. also thank the Deutsche Forschungsgemeinschaft (DFG, German Research Foundation) – Project-ID 405553726 – TRR 270 for funding.

Notes and references

1 V. H. Nowotny, Strukturchemie einiger Verbindungen der Übergangsmetalle mit den elementen C, Si, Ge, Sn, *Prog. Solid State Chem.*, 1971, **5**, 27–70.
2 M. W. Barsoum, The $M_{n+1}AX_n$ Phases: A New Class of Solids: Thermodynamically Stable Nanolaminates, *Prog. Solid State Chem.*, 2000, **28**, 201–281.
3 M. W. Barsoum and T. El-Raghy, The MAX Phases: Unique New Carbide and Nitride Materials, *Am. Sci.*, 2001, **89**, 334–343.
4 N. Haddad, E. Garcia-Caurel, L. Hultman, M. W. Barsoum and G. Hug, Dielectric properties of Ti_2AlC and Ti_2AlN MAX phases: The conductivity anisotropy, *J. Appl. Phys.*, 2008, **104**(2), 023531.
5 T. Flatten, F. Matthes, A. Petruhins, R. Salikhov, U. Wiedwald, M. Farle, J. Rosen, D. E. Bürgler and C. M. Schneider, Direct measurement of anisotropic conductivity in a nanolaminated $(Mn_{0.5}Cr_{0.5})(2)GaC$ thin film, *Appl. Phys. Lett.*, 2019, **115**(9), 094101.
6 M. Jaouen, P. Chartier, T. Cabioch, V. Mauchamp, G. André and M. Viret, Invar Like Behavior of the Cr_2AlC MAX Phase at Low Temperature, *Am. Ceram. Soc.*, 2013, **96**(12), 3872.
7 Z. Liu, T. Waki, Y. Tabata and H. Nakamura, Mn-doping-induced itinerant-electron ferromagnetism in Cr_2GeC, *Phys. Rev. B: Condens. Matter Mater. Phys.*, 2014, **89**, 054435.
8 Z. Liu, T. Waki, Y. Tabata, K. Yuge, H. Nakamura and I. Watanabe, Designer spin systems via inverse statistical mechanics, *Phys. Rev. B: Condens. Matter Mater. Phys.*, 2013, **88**, 134401.
9 J. M. Schneider, Z. Sun, R. Mertens, F. Uestel and R. Ahuja, Ab initio calculations and experimental determination of the structure of Cr_2AlC, *Solid State Commun.*, 2004, **130**, 445.
10 M. Jaouen, M. Bugnet, N. Jaouen, P. Ohresser, V. Mauchamp, T. Cabioch and A. Rogalev, Experimental evidence of Cr magnetic moments at low temperature in Cr_2A (A = Al, Ge)C, *J. Phys.: Condens. Matter*, 2014, **26**, 176002.
11 A. S. Ingason, A. Petruhins, M. Dahlqvist, A. Mockute, B. Alling, L. Hultman, I. A. Abrikosov, P. O. Å. Persson and J. Rosen, A Nanolaminated Magnetic Phase: Mn_2GaC, *Mater. Res. Lett.*, 2014, **2**, 89–93.
12 M. Dahlqvist, A. S. Ingason, B. Alling, F. Magnus, A. Thore, A. Petruhins, A. Mockute, U. B. Arnalds, M. Sahlberg, B. Hjörvarsson, I. A. Abrikosov and J. Rosen, Magnetically driven anisotropic structural changes in the atomic laminate Mn_2GaC, *Phys. Rev. B*, 2016, **93**, 014410.
13 M. Stevens, H. Pazniak, A. Jemiola, M. Felek, M. Farle and U. Wiedwald, Pulsed laser deposition of epitaxial Cr_2AlC MAX phase thin films on MgO(111) and Al_2O_3(0001), *Mater. Res. Lett.*, 2021, **9**(8), 343–349.
14 A. S. Ingason, M. Dahlqvist and J. Rosen, Magnetic MAX phases from theory and experiments; a review, *J. Phys.: Condens. Matter*, 2016, **28**, 433003.
15 M. Dahlqvist, B. Alling, I. A. Abrikosov and J. Rosén, Magnetic nanoscale laminates with tunable exchange coupling from first principles, *Phys. Rev. B: Condens. Matter Mater. Phys.*, 2011, **84**, 220403.
16 Y. L. Du, Z. M. Sun, H. Hashimoto and M. W. Barsoum, Electron correlation effects in the MAX phase Cr_2AlC from first-principles, *J. Appl. Phys.*, 2011, **109**, 063707.

17 M. Dahlqvist, B. Alling and J. Rosén, A critical evaluation of GGA+*U* modeling for atomic, electronic and magnetic structure of $CrCr_2AlC$, Cr_2GaC and Cr_2GeC, *J. Phys.: Condens. Matter*, 2015, **27**, 095601.

18 M. Benouis, Y. Azzaz and M. Ameri, *et al.*, Electronic and Magnetic Properties of Cr_2GeC with GGA + *U* Approximation, *J. Supercond. Novel Magn.*, 2016, **29**, 1267.

19 M. Mattesini and M. Magnuson, Electronic correlation effects in the Cr_2GeC $M_{n+1}AX_n$ phase, *J. Phys.: Condens. Matter*, 2013, **25**, 035601.

20 M. Dahlqvist, Q. Tao, J. Zhou, J. Palisaitis, P. O. Å. Persson and J. Rosen, Theoretical Prediction and Synthesis of a Family of Atomic Laminate Metal Borides with In-Plane Chemical Ordering, *J. Am. Chem. Soc.*, 2020, **142**(43), 18583–18591.

21 M. Dahlqvist and J. Rosen, Predictive theoretical screening of phase stability for chemical order and disorder in quaternary 312 and 413 MAX phases, *Nanoscale*, 2020, **12**(2), 785–794.

22 M. Dahlqvist and J. Rosen, Impact of strain, pressure, and electron correlation on magnetism and crystal structure of Mn_2GaC from first-principles, *Sci. Rep.*, 2020, **10**(1), 11384.

23 M. Dahlqvist, B. Alling and J. Rosén, Stability trends of MAX phases from first principles, *Phys. Rev. B: Condens. Matter Mater. Phys.*, 2010, **81**, 220102(R).

24 V. J. Keast, S. Harris and D. K. Smith, Prediction of the stability of the $M_{n+1}AX_n$ phases from first principles, *Phys. Rev. B: Condens. Matter Mater. Phys.*, 2009, **80**, 214113.

25 G. Kresse and J. Furthmüller, Efficient iterative schemes for *ab initio* total-energy calculations using a plane-wave basis set, *Phys. Rev. B: Condens. Matter Mater. Phys.*, 1996, **54**, 11169.

26 P. E. Blochl, Projector augmented-wave method, *Phys. Rev. B: Condens. Matter Mater. Phys.*, 1994, **50**, 17953.

27 G. Kresse and D. Joubert, From ultrasoft pseudopotentials to the projector augmented-wave method, *Phys. Rev. B: Condens. Matter Mater. Phys.*, 1999, **59**, 1758.

28 J. P. Perdew, K. Burke and M. Ernzerhof, Generalized Gradient Approximation Made Simple, *Phys. Rev. Lett.*, 1996, **77**, 3865.

29 H. J. Monkhorst and J. D. Pack, Special points for Brillouin-zone integrations, *Phys. Rev. B: Solid State*, 1976, **13**, 5188.

30 A. Jain, S. P. Ong, G. Hautier, W. Chen, W. D. Richards, S. Dacek, S. Cholia, D. Gunter, D. Skinner, G. Ceder and K. A. Persson, Commentary: The Materials Project: A materials genome approach to accelerating materials innovation, *APL Mater.*, 2013, **1**, 011002.

31 M. Dahlqvist, B. Alling, I. A. Abrikosov and J. Rosén, Stability trends of MAX phases from first principles, *Phys. Rev. B: Condens. Matter Mater. Phys.*, 2010, **81**(2), 024111.

32 A. Togo and I. Tanaka, First principles phonon calculations in materials science, *Scr. Mater.*, 2015, **108**, 1–5.

33 I. P. Novoselova, A. Petruhins, U. Wiedwald, Á. Sigurdur Ingason, T. Hase, F. Magnus, V. Kapaklis, J. Palisaitis, M. Spasova, M. Farle, J. Rosen and R. Salikhov, Large uniaxial magnetostriction with sign inversion at the first order phase transition in the nanolaminated Mn_2GaC MAX phase, *Sci. Rep.*, 2018, **8**, 2637.

34 H. A. Mook, Magnetic Moment Distribution of Nickel Metal, *Phys. Rev.*, 1966, **148**, 495.

35 E. A. Yelland, S. J. C. Yates, O. Taylor, A. Griffiths, S. M. Hayden and A. Carrington, Ferromagnetic properties of $ZrZn_2$, *Phys. Rev. B: Condens. Matter Mater. Phys.*, 2005, **72**, 184436.

36 D. Ohmer, I. Opahle, H. K. Singh and H. Zhang, Stability predictions of magnetic M_2AX compounds, *J. Phys.: Condens. Matter*, 2019, **31**, 405902.

37 F. Mouhat and F.-X. Coudert, Necessary and sufficient elastic stability conditions in various crystal systems, *Phys. Rev. B: Condens. Matter Mater. Phys.*, 2014, **90**, 224104.

38 A. S. Ingason, A. Mockute, M. Dahlqvist, F. Magnus, S. Olafsson, U. B. Arnalds, B. Alling, I. A. Abrikosov, B. Hjörvarsson, P. O. Å. Persson and J. Rosen, Magnetic Self-Organized Atomic Laminate from First Principles and Thin Film Synthesis, *Phys. Rev. Lett.*, 2013, **110**, 195502.

39 M. W. Barsoum and M. Radovic, Elastic and Mechanical Properties of the MAX Phases, *Annu. Rev. Mater. Res.*, 2011, **41**, 195.

40 J. Wang and Y. Zhou, Dependence of elastic stiffness on electronic band structure of nanolaminate M_2AlC (M = Ti, V, Nb, and Cr) ceramics, *Phys. Rev. B: Condens. Matter Mater. Phys.*, 2004, **69**, 214111.

41 J. Sun, A. Ruzsinszky and J. P. Perdew, Strongly Constrained and Appropriately Normed Semilocal Density Functional, *Phys. Rev. Lett.*, 2015, **115**, 036402.

